Available online at www.sciencedirect.com
ScienceDirect
Physica B 397 (2007) 125–130
PHYSICA B
www.elsevier.com/locate/physb

Spherical neutron polarimetry with MuPAD

M. Janoschek[a,b,*], S. Klimko[a,b,1], R. Gähler[c], B. Roessli[b], P. Böni[a]

[a]Technische Universität München, Physics Department E21, D-85747 Garching, Germany
[b]Laboratory for Neutron Scattering ETHZ & Paul Scherrer Institut, CH-5232 Villigen PSI, Switzerland
[c]Institute Laue Langevin, 6, rue Jules Horowitz, B.P.156, 38042 Grenoble, Cedex 9, France

Abstract

Over the last decade, the systematic application of spherical neutron polarmetry (SNP) has been successfully used to investigate scientific questions which were intractable before, e.g. study of magneto-electric crystals such as $LiCoPO_4$ and $MnGeO_3$. Until now, the only device capable of performing routine SNP measurements at finite scattering angles was CryoPAD (cryogenic polarization analysis device), presented by Tasset et al. in 1989. Recently we demonstrated that an alternative setup named MuPAD (Mu-metal polarization analysis device) based on a zero-field environment produced by highly permeable mu-metal is also feasible. Here we present this new SNP device together with some first results.

PACS: 61.12.−q; 75.80.+q; 75.25.+z

Keywords: Spherical neutron polarimetry; Polarization analysis

1. Introduction

The theory for polarized neutron scattering was developed in the 1960s by various contributors [1–5]. The master equations for this theory namely the Blume–Maleyev equations are given by

$$\sigma \equiv \frac{\mathrm{d}^2\sigma}{\mathrm{d}\Omega\,\mathrm{d}E'} = N + M^y + M^z - P_0^x C + P_0^y R^y + P_0^z R^z \qquad (1)$$

for the polarization dependent partial differential cross-section and

$$\mathbf{P}' = \tilde{\mathbf{P}}\mathbf{P_0} + \mathbf{P}'',$$

$$\sigma\tilde{\mathbf{P}} = \begin{pmatrix} (N - M^y - M^z) & iI^z & -iI^y \\ -iI^z & (N + M^y - M^z) & M_{\mathrm{mix}} \\ iI^y & M_{\mathrm{mix}} & (N - M^y + M^z) \end{pmatrix},$$

$$\sigma\mathbf{P}'' = \begin{pmatrix} C \\ R^y \\ R^z \end{pmatrix}, \qquad (2)$$

for the final polarization vector $\mathbf{P}'$. $\tilde{\mathbf{P}}$ is the polarization tensor, which describes the rotation of the initial polarization vector $\mathbf{P_0}$ in the scattering process and $\mathbf{P}''$ is the polarization created in the scattering process at the sample. All the terms included in Eqs. (1), (2) are only determined by the sample properties that are described by the nuclear structure factor $N_{\mathbf{Q}}$ and the magnetic interaction vector $\mathbf{M}_{\perp\mathbf{Q}}$. They are summarized in Table 1. The nuclear structure factor is given by $N_{\mathbf{Q}} = \sum_i b_i \exp(i\mathbf{Q}\cdot\mathbf{r}_i)$ where $\mathbf{Q}$ is the scattering vector and b_i and $\mathbf{r}_i$ denote the scattering length and position of the individual nuclei, respectively. The magnetic interaction vector is defined as $\mathbf{M}_{\perp\mathbf{Q}} = \hat{\mathbf{Q}} \times (\boldsymbol{\rho}(\mathbf{Q}) \times \hat{\mathbf{Q}})$ where $\boldsymbol{\rho}(\mathbf{Q}) = -2\mu_B \int \boldsymbol{\rho}(\mathbf{r}) \exp(i\mathbf{Q}\cdot\mathbf{r})\,\mathbf{dr}$ is the Fourier transform of the magnetization density $\boldsymbol{\rho}(\mathbf{r})$ of the sample and $\hat{\mathbf{Q}}$ is the normalized scattering vector. We note that we neglected the Debye–Waller factor in the nuclear structure factor and the magnetic interaction vector. Usually the set of polarization axes is defined to have x parallel to the scattering vector $\mathbf{Q}$, z perpendicular

*Corresponding author. Laboratory for Neutron Scattering ETHZ & Paul Scherrer Institut, CH-5232 Villigen PSI, Switzerland.
Tel.: +41 56 3103179; fax: +41 56 3102199.
E-mail address: marc.janoschek@psi.ch (M. Janoschek).
[1]Current institution: DRFMC, CEA-Grenoble, SPSMS-MDN, 17 rue des Martyrs, 38054 Grenoble, Cedex 9, France.

0921-4526/$ - see front matter © 2007 Elsevier B.V. All rights reserved.
doi:10.1016/j.physb.2007.02.074

Table 1
Terms contained in Eqs. (1), (2); $\langle \hat{A}_{\mathbf{Q}} \hat{B}^{\dagger}_{\mathbf{Q}} \rangle_{\omega} = \frac{1}{2\pi\hbar} \int \mathrm{d}t \exp(-\mathrm{i}\omega t) \langle \hat{A}_{\mathbf{Q}} \hat{B}^{\dagger}_{\mathbf{Q}}(t) \rangle$ (e.g. see [6]) are inelastic correlation functions

Item	Correlation functions	Description
N	$\frac{k'}{k}\langle N_{\mathbf{Q}} N^{\dagger}_{\mathbf{Q}} \rangle_{\omega}$	Nuclear contribution
$M^{y/z}$	$r_0^2 \frac{k'}{k}\langle M^{y/z}_{\perp\mathbf{Q}} M^{\dagger y/z}_{\perp\mathbf{Q}} \rangle_{\omega}$	y- and z-components of the magnetic contribution
$R^{y/z}$	$r_0 \frac{k'}{k}\langle N^{\dagger}_{\mathbf{Q}} M^{y/z}_{\perp\mathbf{Q}} \rangle_{\omega} + \langle M^{\dagger y/z}_{\perp\mathbf{Q}} N_{\mathbf{Q}} \rangle_{\omega}$	Real parts of the nuclear-magnetic interference term
$I^{y/z}$	$r_0 \frac{k'}{k}\langle N^{\dagger}_{\mathbf{Q}} M^{y/z}_{\perp\mathbf{Q}} \rangle_{\omega} - \langle M^{\dagger y/z}_{\perp\mathbf{Q}} N_{\mathbf{Q}} \rangle_{\omega}$	Imaginary parts of the nuclear-magnetic interference term
C	$\mathrm{i} r_0^2 \frac{k'}{k}(\langle M^{y}_{\perp\mathbf{Q}} M^{\dagger z}_{\perp\mathbf{Q}} \rangle_{\omega} - \langle M^{z}_{\perp\mathbf{Q}} M^{\dagger y}_{\perp\mathbf{Q}} \rangle_{\omega})$	Chiral contribution
M_{mix}	$r_0^2 \frac{k'}{k}(\langle M^{y}_{\perp\mathbf{Q}} M^{\dagger z}_{\perp\mathbf{Q}} \rangle_{\omega} + \langle M^{z}_{\perp\mathbf{Q}} M^{\dagger y}_{\perp\mathbf{Q}} \rangle_{\omega})$	Mixed magnetic contribution or magnetic-magnetic interference term

$\mathbf{Q}$ is the scattering vector and $\hbar\omega$ the energy transfer; k and k' denote the magnitude of the wavevector of incident and scattered neutrons, respectively; $r_0 = 5.391 \times 10^{-15}$ m is the magnetic scattering length; x, y, z denote the three directions in space, where $x \| \mathbf{Q}$, $y \perp \mathbf{Q}$ in the scattering plane and $z \perp \mathbf{Q}$ out of the scattering plane. By performing the limit $\lim_{t\to\infty} \langle A_{\mathbf{Q}} B^{\dagger}_{\mathbf{Q}}(t) \rangle = \langle A_{\mathbf{Q}} \rangle \langle B^{\dagger}_{\mathbf{Q}} \rangle$ the terms used for elastic scattering can be obtained.

to the scattering plane and y completing the right-handed set. The measured quantity is the polarization matrix, namely the components of the final polarization vector after the scattering process for all three directions of the incident beam polarization,

$$\mathrm{P}_{ij} = (P_{i0}\tilde{P}_{ji} + P'_j)/|\mathbf{P_0}|, \tag{3}$$

where i and j $(i,j = x,y,z)$ denote the directions of the incident and final polarization vectors, respectively. Such a *polarization analysis* experiment gives a lot of additional information compared to just measuring the neutron scattering cross-section in Eq. (1). The additional data can be used to disentangle the different contributions to the scattering cross-section for each point in $(\mathbf{Q},\omega)$-space. In an unpolarized neutron scattering experiment the purely nuclear and purely magnetic contributions are superposed whereas all the other contributions are canceled due to the unpolarized incident beam (see Eq. (1)).

Over the last decade systematic polarization analysis has been used to cope with scientific questions which were intractable before. Some of them are:

- Study of magneto-electric crystals such as $LiCoPO_4$ and $MnGeO_3$ [7]. These compounds rotate the polarization vector in a characteristic way. Measuring this rotation enables to identify the relative population of the magneto-electric domains and to determine the antiferromagnetic structure factors in these compounds and hence the magnetization distribution leading to magneto-electricity.
- Study of non-collinear magnetic structures. For such compounds it is often impossible to distinguish between different possible magnetic structures by other techniques because they are not able to determine the directional information hold in magnetic structure factors. One example is UPtGe [8].
- Investigation of hybrid correlation functions in inelastic neutron scattering in compounds where nuclear and magnetic degrees of freedom or different magnetic degrees of freedom interfere [9].

However, careful control of the polarization vector throughout the whole experimental setup is necessary to perform a polarization analysis experiment as magnetic stray fields in the environment of the instrument may depolarize or rotate the polarization vector. In *classical longitudinal polarization analysis* [10], the depolarization of the beam by residual magnetic fields is prevented by the application of a magnetic guide field along the polarized neutron beam. However, this setup only allows the projection of the final polarization vector onto the direction of the guide field to be determined. Any component of the polarization turned into a direction perpendicular to the guide field upon the scattering process will be depolarized. Hence only the three diagonal terms of the polarization matrix may be determined. However, in order to handle the scientific cases presented above the information of the six off-diagonal terms is additionally needed.

The neutron polarization can be conserved when any residual fields are removed from the sample environment by a zero field chamber. Then any component of the final polarization vector may be determined and the full polarization matrix can be measured. This method is known as *spherical neutron polarimetry* (SNP). Until now CryoPAD (cryogenic polarization analysis device), presented by Tasset et al. [11] in 1989, was the only device to perform routine SNP measurements at finite scattering angles. It is based on a zero field chamber, realized through a double superconducting Meissner-shield.

However, in June 2004 we proved successfully with a prototype of MuPAD (mu-metal polarization analysis device) that an alternative setup based on a zero-field chamber made of highly permeable mu-metal is feasible as well [12].

2. Experimental setup

MuPAD is an experimental setup for SNP using a mu-metal sample chamber to create a zero field environment that conserves the direction of the polarization vector throughout the instrument. The chamber mainly consists of a double layered mu-metal cylinder in which a standard ILL orange cryostat or a FRM-II closed cycle cryostat can be hosted inside the zero field region. With this setup a shielding factor $S = B_{\mathrm{o}}/B_{\mathrm{i}} = 1000$–$3000$ depending on the direction can be achieved inside the zero field chamber,

where B_o and B_i are the fields outside and inside of the chamber, respectively. A magnetic field of 300 mG that is of the order of magnitude of the Earth's magnetic field will reduce the inner magnetic field to a value of the order of $B_i = 0.3$ mG. This can be regarded as a zero field environment for a wide spectrum from hot to very cold neutrons. Thus, the chamber is perfectly suitable to perform a SNP experiment (e.g. neutrons with a wavelength of $\lambda \approx 10$ Å will be turned by $\leqslant 1.2^\circ$ over the length $l = 1.5$ m of the whole chamber). An overview of the chamber is given in Fig. 1.

As a polarized neutron beam cannot traverse a mu-metal layer of several mm thickness without serious losses in intensity and polarization the beam has to enter the zero field chamber through apertures in the mu-metal. To avoid depolarization when the neutrons travel through these apertures and additionally to avoid that magnetic residual fields can penetrate into the zero field chamber through the entrance and exit apertures coupling coils (CCs) are used. Neutrons reach the zero field region with their spins parallel to the guide field of the CC. The transition from the outer guide field to the field of the CC is adiabatic, whereas the transition from the field of the CC into the screened area is strictly nonadiabatic, in order to conserve the spin direction inside the zero field region. The non-adiabatic transition is achieved by passing the neutrons through the wires of the CC; outer stray fields are avoided by a mu-metal yoke closely wrapped around the CC.

Variation of the scattering angle requires a splitting of the double mu-metal cylinder. The gap between the two cylinder parts can be closed section by section by an automated pneumatic system of mu-metal lamellas (see Fig. 1) according to the scattering angle.

To control the polarization vector of the incident and scattered neutrons a set of two *precession coils* (PCs) is used for the incoming and outgoing beam, respectively. They are hosted in two extensions to the zero field chamber, called *arms* in the following. The double mu-metal shields of the arms are connected mechanically and magnetically to the inner and outer mu-metal cylinder of the central chamber, respectively, assuring a zero field environment for these coils (Fig. 1). The arm at the entrance side of MuPAD is fixed with respect to the mu-metal cylinders, whereas the arm at the exit side moves on a rail system together with the opening for the scattered neutrons provided by the automatic mu-metal lamella system. The two CCs are mounted inside the zero field arms (Fig. 1). The PCs are installed inside the zero field arms and special care was taken to ensure that the return fields of the PCs cannot influence the polarization vector of the neutron beam. The rectangular coils have cylindrical coil bodies on which the Al-wire is wound with high precision in order to achieve highly homogeneous inner fields. To ensure a high precision of the winding, grooves were milled into the bodies. The outer field is redirected by a 2 mm thick mu-metal yoke and a secondary 0.65 mm thick mu-metal screen

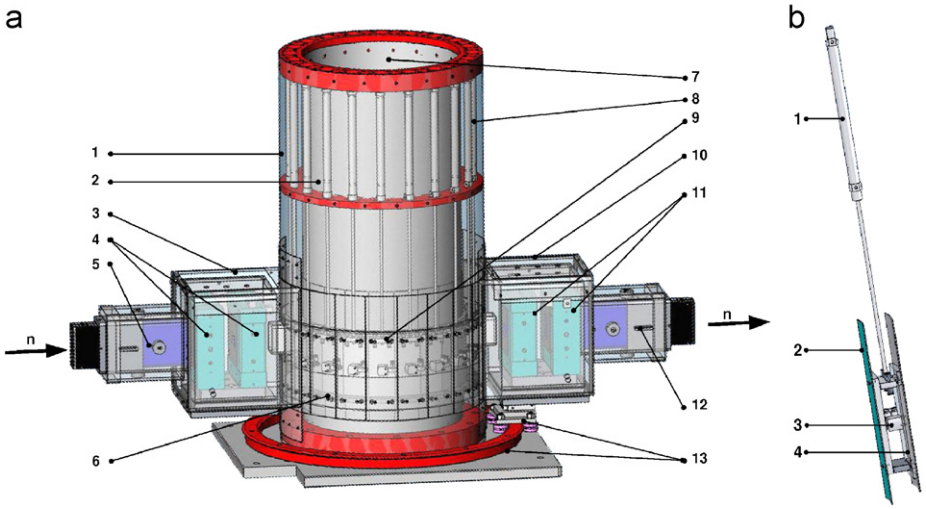

Fig. 1. A technical drawing of the MuPAD device is shown. (a) **n** denotes the direction of the neutron beam. The following details are specified: (1) outer mu-metal shield; (2) inner mu-metal shield; (3) primary fixed arm out of double mu-metal shielding hosting all coils for the incoming neutron beam; (4) precession coils for manipulation of the polarization vector incident on the sample; (5) coupling coil to conserve the polarization vector of the incoming beam; (6) mu-metal lamellas for automatic closure of the beam slit when the scattering vector is changed; (7) top hole for insertion of standard ILL orange or FRM-II closed cycle cryostats; (8) non-magnetic pneumatic cylinders which move mu-metal lamellas; (9) sample position in chamber; (10) secondary moving arm which hosts coils for the outgoing neutron beam; arm is moved together with the host spectrometer; (11) precession coils for manipulation of the final polarization vector; (12) coupling coil to conserve the polarization vector of the outgoing beam; (13) non-magnetic rail system on which the moving secondary arm is mounted. (b) A detailed view of the pneumatic lamella system for automatic closure of the zero field chamber is shown: (1) pneumatic cylinder which moves lamellas up and down; (2) inner mu-metal lamella to magnetically close inner cylinder of chamber; (3) cylinder which spreads inner and outer lamella towards the inner and outer mu-metal shield to assure good magnetic contact when the chamber is closed; (4) outer mu-metal lamella.

(Fig. 2). This reduces the outer residual fields in the beam area to some mG (Fig. 3) and additionally simulates an infinitely long solenoid improving the homogeneity of the inner field. We measured the outer field in the beam axis with a Bartington Single Axis Fluxgate Magnetometer Mag-01H. The measurements show that the PCs can be regarded as ideal field configurations for the neutron wavelengths in mind with non-adiabatic transitions on both sides of the coils (Table 2). This way, a precise control of the polarization vector in all directions is achieved.

The interplay of all precession and CCs is shown in Fig. 4. A neutron beam polarized along the z-direction enters the zero field region via the entrance CC. The two outer PCs control the orientation of the polarization with respect to the scattering plane. The two inner PCs turn the

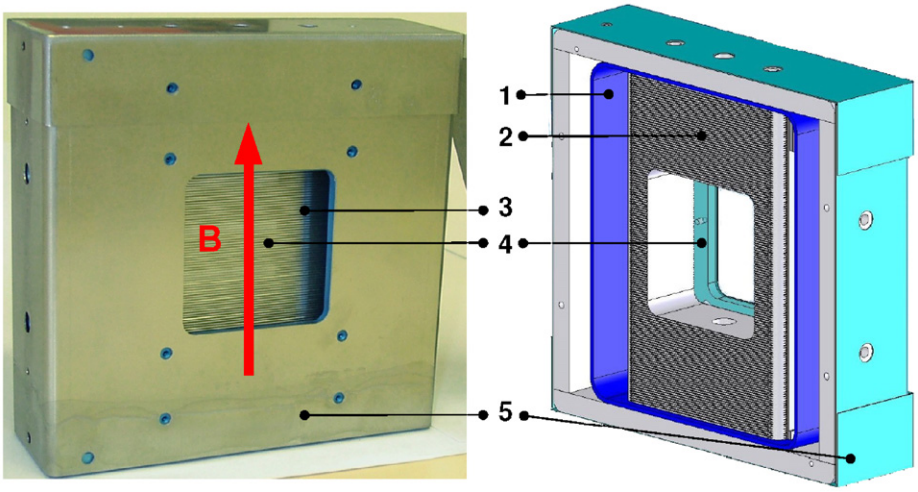

Fig. 2. A MuPAD precession coil is shown: (1) inner 2 mm thick mu-metal yoke; (2) rectangular coil body with grooves to assure high precision winding of wires; (3) Al-wires; (4) window for neutrons; (5) secondary outer mu-metal shields. The arrow denotes the direction of the inner magnetic field.

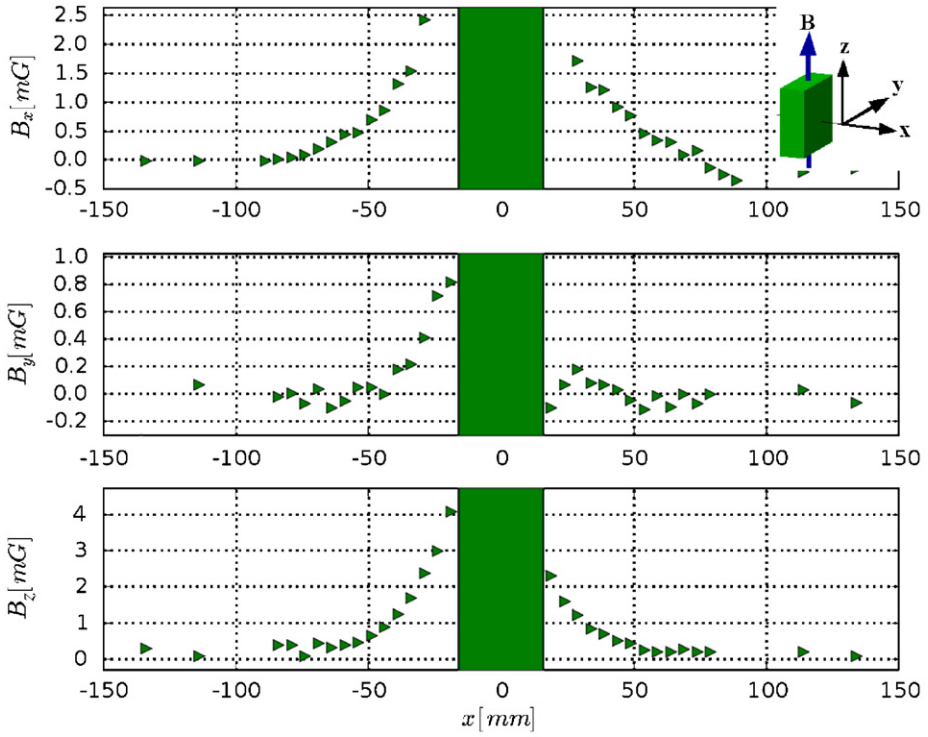

Fig. 3. Residual fields of the precession coils used in MuPAD for an inner field integral of 20.7 G cm corresponding to a $\pi/2$-flip for 1.65 Å neutrons. The shaded area represents the region of the inner field of the coils. The inset in the upper right corner shows the used coordinate frame. The neutron beam traverses the PC in x direction. The integral over the measured fields is shown in Table 2.

polarization within the scattering plane either along and/or perpendicular to **Q**. This setup allows full and precise control of the polarization vector of the neutron beam incident on the sample and of the scattered neutron beam as well.

3. Tests and first results

Two MuPAD devices were built for use at the cold three axis TASP at SINQ in Switzerland [13] and at the very cold neutron beam line MIRA at the FRM-II in Germany, respectively. Tests were performed with neutrons of 2.36 Å wavelength at TASP and 9.7 Å at MIRA.

As an example we show some data that we have recently obtained at MIRA using a MnSi crystal. MnSi is an itinerant-electron ferromagnet with a Curie temperature T_C of about 29 K and an ordered magnetic moment of $0.4\,\mu_B$ on each Mn site. Its magnetic structure in zero field is a long-period ferromagnetic spiral with the propagation vector $(2\pi/a)(\zeta,\zeta\,\zeta)$ with $\zeta = 0.017$ resulting in a period of approximately 180 Å [14,15] along the [1 1 1] direction. SNP measurements on this compound are motivated by the idea by Rößler et al. [16] that the soft longitudinal fluctuations may lead to an intermediate phase in MnSi. In this experiment we used MIRA in the small angle diffraction mode and the sample was adjusted on the instrument to fulfill the Bragg-condition for the magnetic satellite reflection (0.017 0.017 0.017). A typical polarization matrix observed at this peak at $T \simeq 20$ K is shown in Table 3 together with the theoretical matrix expected for the chiral structure of MnSi. The comparison of the matrix elements demonstrates that MuPAD operates well even for long wavelengths up to 9.7 Å where the polarization vector is extremely sensitive to residual fields. Further extensive measurements on this compound will be published in Ref. [17].

Table 2
Field integrals L_i of the residual fields for the MuPAD precession coils for an inner field integral of 20.7 G cm corresponding to a $\pi/2$-flip for 1.65 Å neutrons

	x	y	z
L_i (m Gmm)	120.7	25.5	119.8
ϕ_i (°)	0.05	0.01	0.05

ϕ denotes the rotation of the polarization for the same neutrons due to the residual fields.

4. Conclusion

We constructed and tested an alternative setup to perform routine SNP measurements at finite scattering angles based on a double mu-metal shield and compact PCs with accurately defined field geometry. The tests showed that the measurements can be performed reliably and with good precision ranging from cold to very cold neutrons. Further tests verifying MuPADs compatibility with hot neutrons are foreseen. Therefore we conclude that MuPAD can be successfully used to investigate scientific questions in condensed matter physics which are intractable without the use of the SNP technique.

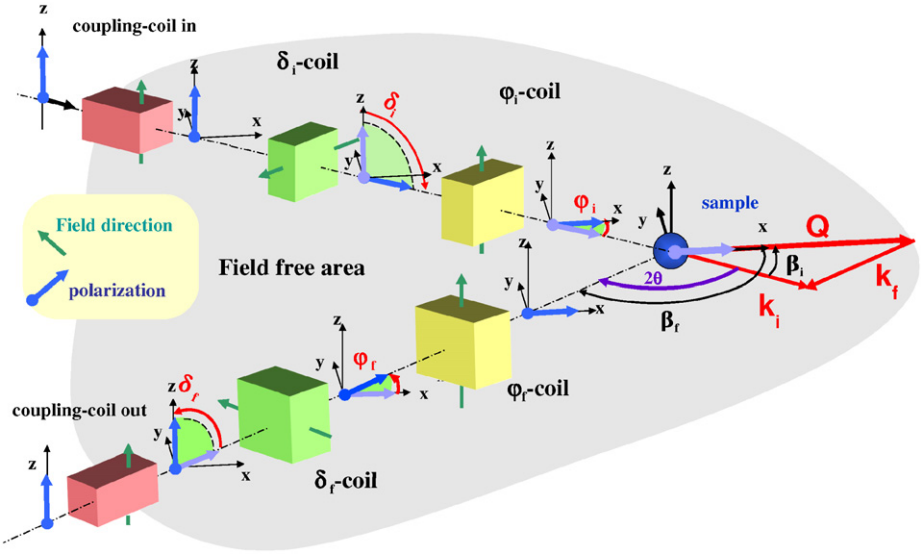

Fig. 4. The setup of MuPAD is shown schematically. A neutron beam polarized along the z-direction enters into the zero field chamber denoted by the grey shaded area through the incident coupling coil. The polarization vector is turned by two precession coils with homogeneous fields perpendicular to each other in order to be aligned along the x-direction. It is scattered on a non-magnetic Bragg peak of a sample (this case was chosen due to the simplicity of the picture). Therefore the polarization vector is not changed during the scattering process. Now the second pair of precession coils downstream of the sample is used to turn the x-component of the final polarization in the direction of the analyser axis (z-axis). This component is guided out of the zero field chamber to the analyser by the exit coupling coil. Thus in this configuration the term P_{xx} of the polarization matrix is measured.

Table 3
Polarization matrix observed on the magnetic satellite reflection (0.017, 0.017, 0.017) is shown together with the expected matrix for this magnetic structure

P_{out}	Measurement			Theory		
	x	y	z	x	y	z
P_{in}						
x	0.836 (7)	0.07 (1)	0.09 (1)	1	0	0
y	0.880 (1)	0.062 (3)	0.091 (3)	1	0	0
z	0.880 (1)	0.059 (3)	0.083 (3)	1	0	0

The elements where the x-component of the final polarization vector is measured are reduced from one due to the finite incident polarization of the neutron beam.

Acknowledgements

We wish to thank C. Pfleiderer, R. Georgii and S. Mühlbauer for support and discussions during the experiment on MnSi. Further, we are particularly grateful to A. Emmert, W. Latscha and R. Bürge for assistance, advices and discussions during the construction process of MuPAD. This work is based on experiments performed at the FRM-II research reactor, Technical University of Munich, Germany and at the Swiss spallation neutron source SINQ, Paul Scherrer Institute, Villigen, Switzerland.

References

[1] Y.A. Izyumov, S. Maleyev, Sov. Phys. JETP 14 (1962) 1668.
[2] M. Blume, Phys. Rev. 130 (1963) 1670.
[3] Y.A. Izyumov, Sov. Phys. Usp 16 (1963) 359.
[4] M. Blume, Phys. Rev. 133 (1964) A1366.
[5] R.I. Schermer, M. Blume, Phys. Rev. 166 (1968) 554.
[6] S.V. Maleyev, Physica B 267–268 (1999) 236.
[7] P.J. Brown, J.B. Forsyth, F. Tasset, Solid State Sci. 7 (2005) 682.
[8] D. Mannix, S. Coad, G.H. Lander, J. Rebizant, P.J. Brown, J.A. Paixão, S. Landgridge, S. Kawamata, Y. Yamaguchi, Phys. Rev. B. 62 (6) (2000) 3801.
[9] L.P. Regnault, H. Rønnow, C. Boullier, J. Lorenzo, C. Marin, Physica B 345 (2004) 111.
[10] R.M. Moon, T. Riste, W. Koehler, Phys. Rev. 181 (1969) 920.
[11] F. Tasset, Physica B 156–157 (1989) 627.
[12] M. Janoschek, Master's Thesis, Technical University Munich ⟨http://mupad.wired-things.de⟩, 2004.
[13] F. Semadeni, B. Roessli, P. Böni, Physica B 297 (152) (2001) 152.
[14] G. Shirane, R. Cowley, C. Majkrzak, J. Sokoloff, B. Pagonis, C.H. Perry, Y. Ishikawa, Phys. Rev. B 28 (1983) 6251.
[15] B. Roessli, P. Böni, W. Fischer, Y. Endoh, Phys. Rev. Lett. 88 (2002) 237204.
[16] U.K. Rößler, A.N. Bogdanov, C. Pfleiderer, Nature 442 (2006) 797.
[17] M. Janoschek, C. Pfleiderer, P. Böni, to be published.